THE JOURNAL OF PHYSICAL CHEMISTRY C

Article

pubs.acs.org/JPCC

Critical Size for Bulk-to-Discrete Transition in 2D Aliphatic Layers: Abrupt Size Effect Observed via Calorimetry and Solid-State ^{13}C NMR

Zichao Ye,[†,⊥] Lito P. de la Rama,[†,∥] Mikhail Y. Efremov,[‡] Andre Sutrisno,[§] and Leslie H. Allen*[,†]

[†]Department of Materials Science and Engineering, Frederick-Seitz Materials Research Laboratory, Coordinated Science Laboratory, University of Illinois at Urbana—Champaign, Urbana, Illinois 61801, United States

[‡]College of Engineering, University of Wisconsin—Madison, Madison, Wisconsin 53706, United States

[§]NMR/EPR Laboratory, School of Chemical Sciences, University of Illinois at Urbana—Champaign, Urbana, Illinois 61801, United States

Supporting Information

ABSTRACT: Anomalous changes of physical properties are observed in an abrupt bulk-to-discrete transition in layered silver alkanethiolate (AgSCn, n = 1−16). A critical chain length of n_{cr} = 7 marks the sharp boundary between the bulk (uniform, $n \geq 7$) and discrete (individualistic, $n \leq 6$) forms of AgSCn. Solid-state ^{13}C NMR analysis reveals that none of the carbons share identical chemical environment in the discrete range, making each AgSCn with n = 2−6 uniquely different material, even though the crystal structure is preserved throughout. Extraordinary changes of thermodynamic properties appearing at this bulk-to-discrete transition include ∼500% increases of melting enthalpy (ΔH_m), ∼50 °C increases of melting point (T_m), and an atypical transition between size-dependent T_m depression and T_m enhancement. We develop a new comprehensive Gibbs−Thomson model with piecewise excess free energy (ΔG_{excess}) to predict the nature of the abrupt size effect melting. A new 3D spatial model is constructed to divide the aliphatic chains of AgSCn into three bulk or discrete segments: (a) tail segment containing three carbons, (b) head segment containing two carbons, and (c) bulk mid-chain segment containing (n − 5) carbons. Odd/even effect of T_m and ΔH_m is described by a constant ΔG_{excess} over the entire chain length range of AgSCn and is exclusively attributed to the localized tail segment. Bulk-to-discrete transition occurs when material properties are dominated by the discrete head and tail segments at $n < n_{cr}$. Values of n_{cr} are independently measured by both calorimetry and ^{13}C NMR. This analysis is generalized to other aliphatic layers including n-alkanes with $n_{cr} \approx 11$. This work is seminal to the design of novel aliphatic layers with tailorable properties (e.g., T_m) and has applications in molecular electronics and biophysics.

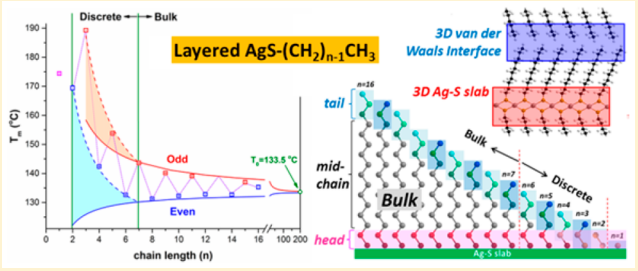

1. INTRODUCTION

Materials often exhibit exotic properties because of "discrete regions", regions that have different chemical environment from the remaining part of the system. Material at the first level is treated as a uniform "bulk" with single sets of intrinsic and extrinsic characteristics; the next level incorporates finer details of the system by segmenting it with discrete regions, including interfaces (e.g., lamella mating boundaries),[1−4] surfaces (e.g., nanoparticle spheres),[5−9] and defects (e.g., gauche kinks).[10] The effect of these discrete regions is highlighted by material miniaturization. At extremely small scale lengths (<10 nm), properties of the "whole" object (e.g., melting,[7,11] lattice structure,[12,13] bandgap,[14,15] conductivity,[16] optical[17]) are dominated by the nature of discrete regions.

Materials with ultimate size scales, such as graphene,[18] 2D metal dichalcogenides,[19] layered silver alkanethiolate (AgSCn),[2,20] and clusters of countable atoms[21−24] are currently of growing scientific and technological interest. These are examples where the discrete regions comprise the majority of the materials.

Size-dependent melting (T_m) of nanoparticles[7,11,25−28] sets an example of progressive transition from materials of mostly bulk to those dominated by discrete regions (bulk-to-discrete transition). Melting enthalpy (ΔH_m) of Sn nanoparticles disappears at a critical radius of ∼25 Å (Figure 1a).[11] Bulk properties are only defined in particles larger than the critical size, with the inner bulk core embedded in the discrete surface overlayers,[5,7,29,30] whereas the entire system is occupied by the discrete region below the critical radius. Chemical environment (bonding, mobility, packing) of the atoms in the discrete surface may be completely different from that of the bulk core.

This work is focused on a systematic study of 2D aliphatic layers near the critical size. AgSCn (n = 1−16) is chosen as the model system due to its importance in biophysics[31,32] and flexibility of designing new materials from interface tailoring.[33,34] A new synthesis method[13] developed in our group creates highly ordered metal thiolate layers with extremely

Received: April 19, 2017
Revised: June 5, 2017
Published: June 5, 2017

DOI: 10.1021/acs.jpcc.7b03693
J. Phys. Chem. C 2017, 121, 13916−13929

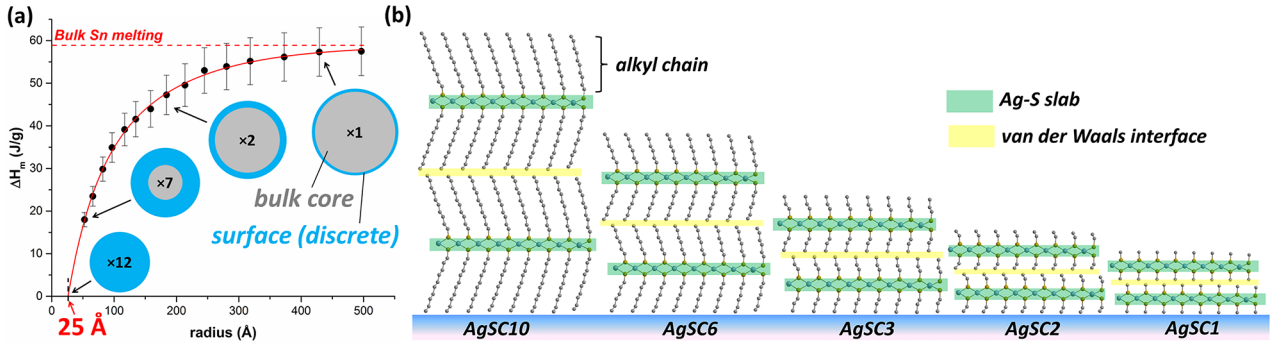

Figure 1. (a) Plot shows ΔH_m as a function of Sn nanoparticle radius.[11] Schematics of nanoparticles (not to scale, numbers such as "×12" refer to the schematic magnification of the particle) show that the surface regions become dominant as particle size reduces. ΔH_m vanishes at/below radius of ~25 Å. (b) Schematics illustrate the gradual shortening of the chain length of long chain AgSC*n* (e.g., n = 10) to access lamellae with extremely short chain lengths (n = 1−5). An AgSC*n* layer consists of an Ag−S slab with alkyl chains extending both sides. The interlayer interfaces (yellow) and the Ag−S slabs (green) act as discrete regions in AgSC*n*.

short chain lengths (n = 1−5), which were previously considered almost disordered.[17,35]

We access the discrete regions (Ag−S slabs and van der Waals interlayer interfaces) of AgSC*n* lamellae by gradually shortening the aliphatic chain length (Figure 1b). Sharp anomalies begin to present below a critical chain length of n_{cr} ≈ 7. Parallel alkyl chains are bonded laterally with van der Waals force. Chain melting of AgSC*n* is essentially an order−disorder phase transition, in which gauche defects are accumulated in the initially all-trans alkyl chains,[2,36−40] while the Ag−S slabs are intact.[38−40]

Biological molecules like phospholipids[32] (building blocks of cell membranes) have similar structures to AgSC*n* layers. Lamellar chain melting of lipids[41−44] is of particular interest regarding lipid−protein interactions,[32] membrane-expanding drugs,[45] and lung alveolar dynamics.[46] T_m of lipids also depends on the nature of discrete regions, including the head functional groups and the membrane surfaces.[31,47]

Solid-state ^{13}C nuclear magnetic resonance (NMR)[38,48−56] is used in this work to measure the chemical environment and tag/probe the positions of each atom located within the discrete regions. It is highly sensitive to the miniscule localized variations of individual carbons.

Calorimetry measurements allow us to quantify the composite (spatially averaged but not localized) thermodynamic properties of the whole lamellar system.

In this paper, we semiquantitatively link the global (calorimetry) and the local (NMR) characteristics of atoms within the discrete regions of aliphatic layers. We observe an abrupt bulk-to-discrete transition occurring at a critical size of n_{cr} = 7 in AgSC*n* lamellae. A new spatial model is established to divide the alkyl chains into head, tail, and bulk mid-chain segments. An internal phenomenon (odd/even effect) is detected in both the melting and NMR chemical shift of AgSC*n* and is exclusively attributed to the nature of tail segment, within a new 3D representation of the interface region. A new comprehensive Gibbs−Thomson (GT) model is developed to piecewise couple the excess free energy (ΔG_{excess}) to predict the anomalous size-dependent melting above/at/below the critical size. This methodology is generalized to other aliphatic layers with unique discrete regions, including *n*-alkanes with n_{cr} ≈ 11.

2. EXPERIMENTAL SECTION

2.1. Synthesis. AgSC*n* (n = 1−16) lamellae in this work are synthesized by a modified solution method reported in our prior paper.[13,40] In step 1, silver salt is mixed with *n*-alkanethiols in acetonitrile to produce AgSC*n* precipitation. In step 2, the as-synthesized AgSC*n* is Ostwald ripened or recrystallized in hot toluene to improve structure ordering. All samples are multilayer single crystals (n = 1−16) with formulas stoichiometry, all-trans alkyl chains, well-registered interlayer interfaces, and highly ordered lattice structures.[13] The whole synthesis procedure is detailed in the Supporting Information.

2.2. Solid-State ^{13}C Nuclear Magnetic Resonance (NMR). ^{13}C NMR spectroscopy is applied to measure the chemical environment of carbons along the alkyl chains in AgSC*n* (n = 1−16). All the spectra are obtained using a Varian Unity Inova 300 NMR spectrometer (7.05 T), operating at a resonance frequency of ν_0 (^{13}C) = 75.47 MHz at room temperature. A Varian/Chemagnetics 4 mm double-resonance APEX HX magic-angle spinning (MAS) probe is used for all MAS experiments under a spinning rate of 10 kHz and TPPM ^{1}H decoupling. The samples are finely ground and packed into 4 mm o.d. standard zirconia rotors.

Experimental carbon chemical shift referencing, pulse calibration, and cross-polarization condition are done using powdered hexamethylbenzene (HMB), which has a chemical shift of 17.3 ppm (for the methyl peak) relative to the primary standard, TMS at 0 ppm. For cross-polarization MAS (CPMAS) experiments, the ^{1}H 90° pulse width is 2.25 μs, the contact time used is 1 ms, and the recycle delay is set to 2 s. Generally, 600−1000 scans are acquired with an acquisition time of 40 ms for each spectrum to get decent signal-to-noise ratio. Typical line broadening applied for most spectra is 25 Hz with 2 or 3 zero fills done to get 8192 data points in the frequency domain spectra.

Direct-polarization MAS (DPMAS) is used to measure the carbon spin−lattice relaxation times (T_1) of carbon. The 90° pulse width is 2.5 μs, a recycle delay of 30−110 s is used, and 200−2000 scans are collected for each spectrum. T_1 is measured using the standard inversion−recovery sequence (π−τ_1−π/2−τ_2−acq) using recycle delays that are at least 5 times the longest carbon T_1 values to ensure full equilibrium magnetization. The time between the 180° inversion pulse and the 90° pulse (i.e., τ_1 or recovery time) is incremented from very short delays (generally in μs) to longer delays (up to

DOI: 10.1021/acs.jpcc.7b03693
J. Phys. Chem. C 2017, 121, 13916−13929

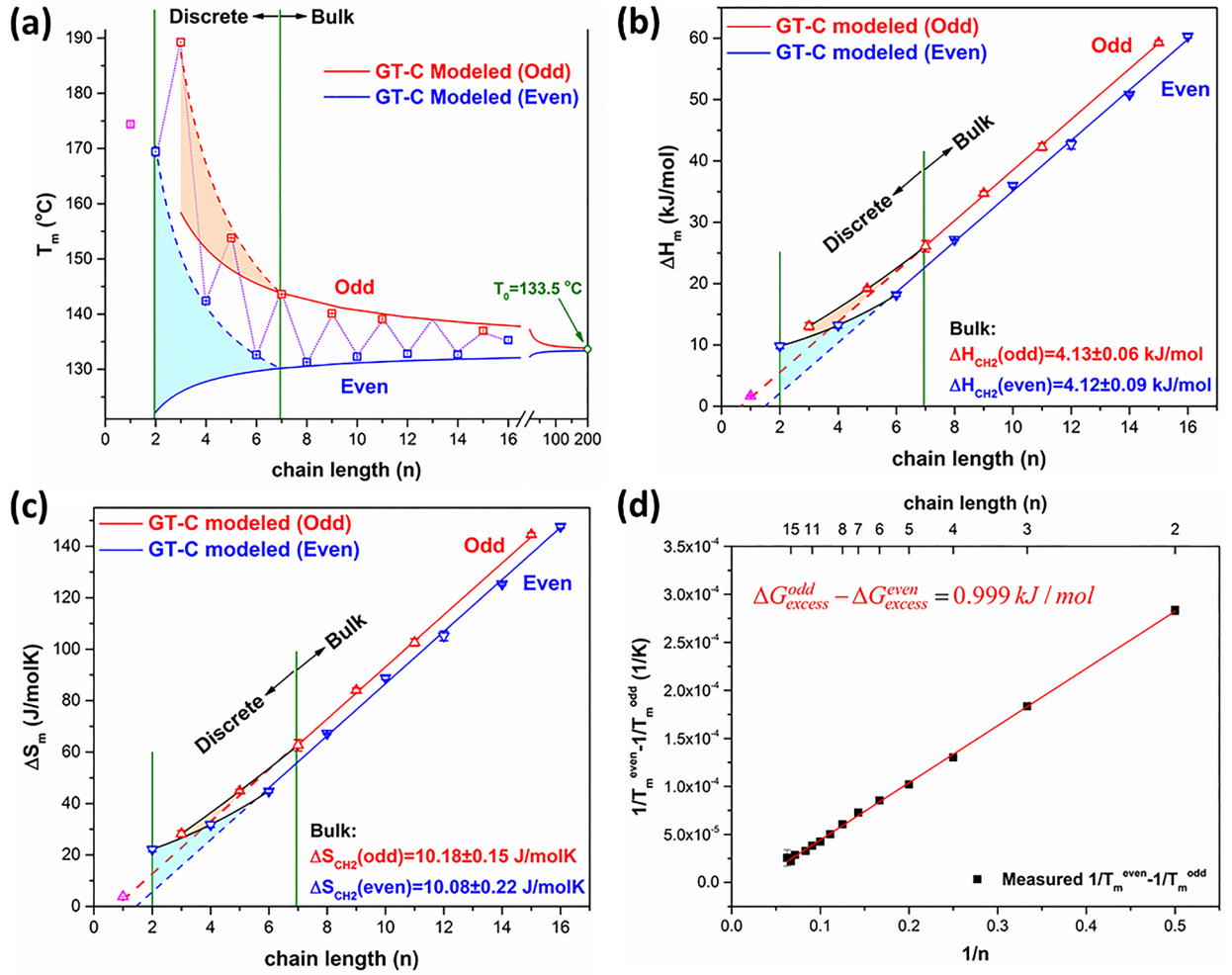

Figure 2. (a), (b), and (c) show the chain melting T_m, ΔH_m, and ΔS_m of AgSCn (n = 1−16) as a function of chain length, respectively. The solid red and blue curves refer to the GT-C model. The orange and cyan shades illustrate the magnitude of the short-chain effect. (d) Plot shows the linear fitting between $(1/T_m^{even} - 1/T_m^{odd})$ and $1/n$. The method used to obtain the data is described in the Supporting Information (Figure S-4).

seconds, depending on which carbon site). The spectra start out inverted (negative peaks), and as the recovery time is increased, the signals will recover their magnetization and the typical "positive" spectra are obtained. The T_1 relaxation curves are then fitted using the data analysis module in MestReNova version 8.1, using the "three parameter exponential fit": $y = B + F\exp(-xG)$.

2.3. Differential Scanning Calorimetry (DSC). Melting properties (melting point T_m, molar melting enthalpy ΔH_m, molar melting entropy ΔS_m) of AgSCn crystals are systematically investigated using a PerkinElmer Standard DSC-4000 with aluminum sample pans. It has a temperature resolution of 0.1 °C and a calorimetric enthalpy error of 2%. The heating and cooling rates of all the scans are set to be 10 °C/min. The instrument is precalibrated using standard indium and zinc metals before real measurements.[57] Experiments are conducted in N_2 atmosphere. The real time heat capacity (C_p) of the sample is calculated by dividing the collected heat flow over scanning rate. The obtained C_p vs T curves are used to determine T_m (peak position) and ΔH_m (peak area over sample weight) of samples. ΔS_m is calculated by dividing ΔH_m over T_m.

3. RESULTS

3.1. Size-Dependent Chain Melting. Calorimetric C_p vs T curves of AgSCn (n = 1−16) lamellae are illustrated in Figure S-1 in Supporting Information. Each curve shows only one phase transition peak that represents chain melting. All transitions are reversible under multiple heating/cooling cycles (ΔH_m varies within 10%), except for AgSC1. Details of the reversibility are given in the Supporting Information (Figures S-2 and S-3).

Parts a−c of Figure 2 show the T_m, ΔH_m, and ΔS_m of AgSCn (n = 1−16) crystals as a function of chain length, respectively. For the purpose of this paper, we denote three stoichiometry ranges of AgSCn: AgSC1, discrete (short chain) AgSCn (n = 2−6), and bulk (long chain) AgSCn ($n \geq 7$). AgSCn (n = 2−16) compounds categorized in bulk and discrete ranges are the focus of this work. The following four key features are observed by the calorimetric measurement:

(1) Bulk AgSCn ($n \geq 7$) follows the classical GT model[4,58−62] with constant values of ΔG_{excess}.
(2) Odd/even effect melting is observed and follows the GT model with constant values of ΔG_{excess} over the entire range of chain length (n = 2−16).
(3) Melting of discrete AgSCn (n = 2−6) requires a new feature in the classical GT model: variable values of ΔG_{excess}.
(4) AgSC1 must be considered as a separate material due to a different crystal structure.

DOI: 10.1021/acs.jpcc.7b03693
J. Phys. Chem. C 2017, 121, 13916−13929

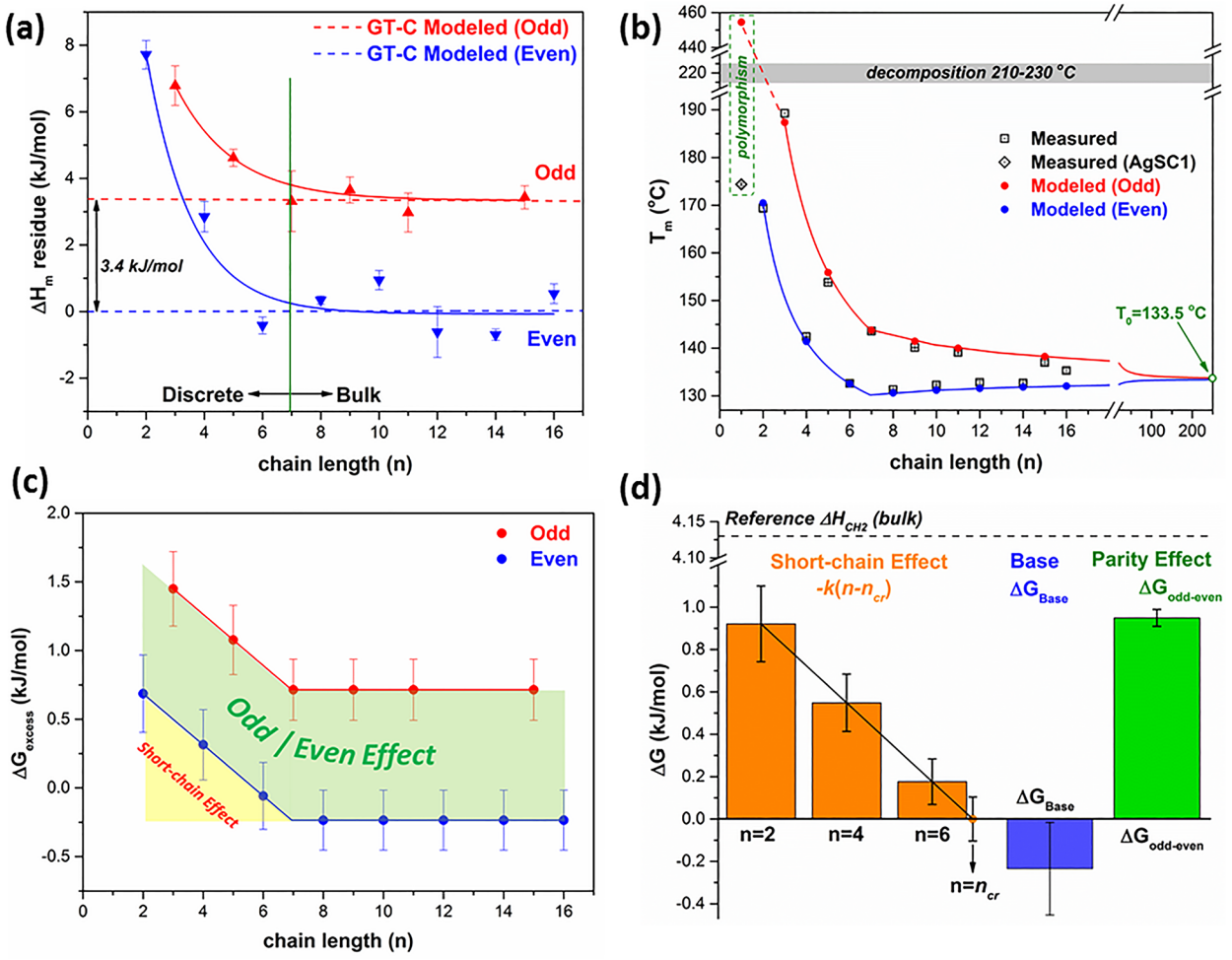

Figure 3. (a) Plot shows the deviations (residues) of ΔH_m (Figure 2b) from that of the linear fitting of either odd or even chain AgSCn with $n \geq 7$. ΔH_m residue for the fitting of even chain lamellae ($n \geq 7$, blue dashed line) is set to be zero. (b) Plot compares the measured T_m (same as Figure 2a) and the GT-COM modeled T_m as a function chain length for AgSCn (n = 2−16). The gray region denotes the decomposition temperature of AgSCn. (c) Plot shows the modeled excess free energy (ΔG_{excess}) as a function of chain length. (d) Bar plot compares the magnitude of the three terms of excess free energy contributed from the short-chain effect (yellow), the base energy (blue), and the parity effect (green). The dashed line refers to bulk ΔH_{CH_2} as a reference.

3.1.1. Long Chain Melting ($n \geq 7$): Classical GT Size Effect. Measured values of T_m, ΔH_m, and ΔS_m (Figure 2a−c) for long chain AgSCn ($n > 6$) are consistent with "bulk" values from literature within experimental errors.[2,36,38,40,57] All T_m values converge to T_0 = 133.5 °C (obtained in section 3.2) for extremely long chains ($n \to \infty$). Melting properties (T_m, ΔH_m, ΔS_m) in this region depend on two separate and independent attributes: chain length and chain parity.

Size-dependent melting[58] is a universal rule that occurs in all materials, including metal particles[5,26,59,62,63] and polymeric layers.[1,4,60,61,64,65] The effect can be described quantitatively by the classical GT model,[58] with the form of eq 1 specifically used in aliphatic materials:[61,66]

$$\frac{1}{T_m} = \frac{1}{T_0}\left[1 - \frac{\Delta G_{excess}}{\Delta H_{CH_2} n}\right] \quad (1)$$

where "n" is chain length and ΔH_{CH_2} is the bulk melting enthalpy per CH_2 group (its value is measured later in this section). For the purpose of this work, eq 1 is labeled as GT-C model due to constant values of ΔG_{excess}, whereas GT-COM model refers to the new comprehensive GT model and contains both variable and constant ΔG_{excess}. Size effect melting of most materials can be explained by the GT-C model, including metals (e.g., Sn,[11] In [7]) and polyethylene.[1,60]

In this work, GT-C model is applied separately to the melting of odd and even chain AgSCn but is valid only for a certain range of chain length. Figure 2a (solid red and blue curves) shows the model works well for long chain crystals with chain lengths exceeding a critical size of n_{cr} = 7.

In this regime of $n \geq n_{cr}$, ΔH_m (Figure 2b) and ΔS_m (Figure 2c) values scale linearly with chain length in analog with Vegard's law.[67−69] The differential values of enthalpy per CH_2 unit are identical for odd (4.13 ± 0.06 kJ/mol) and even (4.12 ± 0.09 kJ/mol) chain AgSCn ($n \geq 7$). This is consistent with the ones obtained from bulk polyethylene (ΔH_{CH_2} = 3.9−4.1 kJ/mol)[1,70] and long chain n-alkanes (n = 11−100, $\Delta H_{CH_2}^{Odd}$ = 4.18 ± 0.08 kJ/mol, $\Delta H_{CH_2}^{Even}$ = 4.14 ± 0.01 kJ/mol).[71] Similarly, melting entropy per CH_2 group (ΔS_{CH_2}) obtained from the linear fittings of long chain AgSCn ($n \geq 7$) is 10.18 ± 0.15 J/(mol K) and 10.08 ± 0.22 J/(mol K) for odd and even chain crystals, respectively. These values agree with others' results of 7−12 J/(mol K).[40] The y-intercepts of the ΔH_m and

DOI: 10.1021/acs.jpcc.7b03693
J. Phys. Chem. C 2017, 121, 13916−13929

ΔS_m plots represent the excess enthalpy and excess entropy associated with melting and are utilized to estimate the excess free energy: $\Delta G_{excess}{}^{odd} \approx 0.71$ kJ/mol and $\Delta G_{excess}{}^{even} \approx -0.30$ kJ/mol.

Interestingly, the direction of size effect melting is opposite between odd and even chain AgSCn ($n \geq 7$, Figure 2a). This observation shows the coexistence of melting point depression (even chain) and melting point enhancement (odd chain) in a single material system. T_m decreases for even chains while it increases for odd chains as chain length shortens, with their corresponding values of ΔG_{excess} showing opposite signs ($\pm$) in the GT-C model. The difference in the packing of lamellae interfaces for odd and even chain crystals is responsible for this effect.[2]

3.1.2. Odd/Even Parity Effect. Strong odd/even effect (parity of chain length) is observed in all calorimetry data (Figure 2a–c, T_m, ΔH_m, ΔS_m) for multilayer AgSCn (n = 2–16). This parity effect was also observed in our prior works for the layer thickness of the same lamellae[2,13] as well as T_m of 2-layer, 3-layer, and 4-layer AgSCn ($n \geq 7$).[2] In contrast, the odd/even effect is weak, if at all present, in our previous multilayer samples (poor crystallinity),[2] due to the limitation of the growth technique, as compared to the improved synthesis route[13] in this work.

The parity effect for the T_m of AgSCn (n = 2–16) is analyzed in Figure 2d and eq 2 by differentially applying the GT-C model to odd and even chain crystals:

$$\frac{1}{T_m^{even}} - \frac{1}{T_m^{odd}} = \frac{1}{T_0}\frac{\Delta G_{excess}^{odd} - \Delta G_{excess}^{even}}{\Delta H_{CH_2} n} \quad (2)$$

Surprisingly, the parity effect is independent of the attribute of AgSCn that is responsible for the short-chain effect (see section 3.1.3). The excess free energy difference in eq 2 is found to be a constant ($\Delta G_{excess}^{odd} - \Delta G_{excess}^{even} = 0.999 \pm 0.017$ kJ/mol) for all chain lengths, including discrete AgSCn (n = 2–6), as illustrated by the linear fitting of Figure 2d. This result occurs despite the observation that both ΔG_{excess}^{odd} and ΔG_{excess}^{even} vary considerably in the short chain regime ($n \leq 6$, section 3.2); yet their difference always remains constant!

3.1.3. Short-Chain Effect below the Critical Size. T_m, ΔH_m, and ΔS_m of AgSCn present huge nonlinear deviations as chain length is smaller than the critical size $n_{cr} = 7$. These abrupt deviations are highlighted in the shaded areas (orange and cyan) in Figure 2a–c. We name the phenomenon responsible for such deviation as "short-chain effect".

Among the deviations, the measured T_m of AgSC2 is ~50 °C (Figure 2a) higher than that expected from the GT-C model on long chain AgSCn ($n \geq 7$), while its ΔH_m is ~500% (Figure 2b) of the modeled value. Expected from the dashed extrapolation of even chain enthalpy (Figure 2b), AgSC2 should be almost completely melted with a ΔH_m of ~2.1 kJ/mol ($\Delta H_m < \Delta H_{CH_2}$), which, however, is 7.7 kJ/mol smaller than the measured value. The 7.7 kJ/mol difference is visualized in Figure 3a and is equivalent to the melting of two bulk CH_2 groups ($2\Delta H_{CH_2} \approx 8.2$ kJ/mol). Another feature of the short-chain effect is the inflection point observed in Figure 2a for even chain AgSCn melting point depression at $n > n_{cr}$ and melting point enhancement at $n < n_{cr}$ ($n_{cr} = 7$).

Clearly there is a fundamental change in the material as the molecule size crosses the critical length (n_{cr}). This change is molecularly abrupt, occurring within one CH_2 unit. One might expect this abruptness is attributed to the change of lattice structure, as observed in AgSC1 (section 3.1.4). However, all structure parameters, including layer thickness (XRD)[2,13] and intralayer lattice constants (within ±2%, electron diffraction),[13] indicate that the crystal structure of AgSCn is preserved throughout the entire chain length range of n = 2–16.

To further analyze the short-chain effect, we (1) establish the new GT-COM model based on the classical GT-C model[61] and the experimental data and (2) observe the local environment and dynamics of each individual carbon within the critical size of $n_{cr} = 7$, using ^{13}C NMR.

3.1.4. AgSC1: The Unique Outlier in AgSCn. AgSC1 must be considered as a unique compound in AgSCn family due to its different crystal structure.[13] Parts a–c of Figure 2a show that T_m, ΔH_m, and ΔS_m of AgSC1 do not follow the trend of all other AgSCn (n = 2–16).

By application of the GT-COM model (section 3.2), AgSC1 is expected to melt at T_m = 454 °C (Figure 3b), which is 280 °C higher than the measured T_m = 174 °C. This model expected value is also ~230 °C higher than the decomposition temperature[13] (210–230 °C, Figure 3b), which implies that AgSC1 is predicted to decompose before it can melt.

3.2. Comprehensive Gibbs–Thomson (GT-COM) Model. Using a constant ΔG_{excess} to explain the size effect melting over the entire chain length range of AgSCn is not consistent with the measurements. The occurrence of the short-chain effect and the parity effect prompts the need for a new GT model: the GT-COM model. One might argue that the short-chain effect can be predicted by the more accurate second order expansion of the GT-C model,[72] yet calculations rebut this possibility, as detailed in the Supporting Information (Table S-1).

We propose a simple and functionally incremental change of ΔG_{excess} for the purpose of modeling the short-chain effect and the parity effect with minimum number of parameters. Below the critical length of n_{cr}, the excess free energy of AgSCn varies linearly (at rate k) as a function of chain length. The preserved odd/even alternation shown in Figure 2d inspires a constant representation of the parity effect: $\Delta G_{odd-even}$. The excess free energy (ΔG_{Base}) of even chain AgSCn above the critical length ($n \geq 7$) is set as the baseline for all lamellae. Therefore, the alterable excess free energy of AgSCn (n = 2–16) in the GT-COM model is expressed as follows:

$$\Delta G_{excess}^{even} = \begin{cases} \Delta G_{Base} - k(n - n_{cr}), & \text{if } n \leq n_{cr} \\ \Delta G_{Base}, & \text{if } n > n_{cr} \end{cases}$$

$$\Delta G_{excess}^{odd} = \begin{cases} \Delta G_{Base} - k(n - n_{cr}) + \Delta G_{odd-even}, & \text{if } n \leq n_{cr} \\ \Delta G_{Base} + \Delta G_{odd-even}, & \text{if } n > n_{cr} \end{cases} \quad (3)$$

On the basis of eq 3, the entire data of measured T_m (Figure 2a) are separated piecewise by partitioning them into four categories: odd chain, even chain, long chain ($n \geq n_{cr}$), and short chain ($n < n_{cr}$). Fitting is conducted by replacing the ΔG_{excess} term in eq 1 with eq 3 to search for the values of T_0, ΔG_{Base}, $\Delta G_{odd-even}$, k, and n_{cr}. The fitting procedure is detailed in the Supporting Information. The calculated parameters are given in Table 1.

The GT-COM model yields an excellent fit of the experimental T_m data, as shown in Figure 3b. The fitted T_0 agrees with our prior result,[2] and n_{cr} equals the experimental value of $n_{cr} = 7$ (section 3.1.1). The modeled $\Delta G_{odd-even}$ is

DOI: 10.1021/acs.jpcc.7b03693
J. Phys. Chem. C 2017, 121, 13916–13929

Table 1. Calculated Values of the Fitting Parameters

parameter	value
T_0	133.5 ± 2.2 °C
ΔG_{Base}	−0.234 ± 0.218 kJ/mol
$\Delta G_{odd-even}$	0.949 ± 0.040 kJ/mol
n_{cr}	6.95 ± 0.56
k	−0.186 ± 0.029 kJ/mol

consistent with the one measured in Figure 2d. In contrast, $\Delta G_{odd-even}$ estimated from our previous work equals only 0.04 kJ/mol, due to the limitation of the synthesis method (poor crystallinity).[2]

Figure 3c presents the values of ΔG_{excess} over the entire chain length range (n = 2−16). This model deconvolutes the short-chain effect ($-k(n - n_{cr})$, Figure 3c yellow region) and the parity effect ($\Delta G_{odd-even}$, Figure 3c green region) from the GT-C baseline (ΔG_{Base}). The comparison of these three contributions to ΔG_{excess} is visualized in Figure 3d. Superposition of these terms well predicts the overall size effect melting of AgSCn; melting of AgSC3 ($n < n_{cr}$) has three aspects of excess free energy superimposed upon the bulk CH_2 melting (dashed line in Figure 3d). At $n = n_{cr}$, the short-chain effect disappears, as is shown by the orange point in Figure 3d. At $n \geq n_{cr}$, the GT-COM model is simply the GT-C model. This new model is generalized to other aliphatic layers with short-chain effect, including n-alkanes, in section 3.6.

3.3. Size Effect Observed in ^{13}C NMR. Calorimetry is a powerful technique to determine the composite thermodynamic properties (T_m, ΔH_m). However, "melting" is a collective process: the sum of contributions from multiple atoms/groups with different (perhaps unique) chemical structures/environment and bonding attributes. The shortfall of calorimetry in this work is that AgSCn expresses only a single melting peak that cannot be deconvoluted into separate contributions of ΔH_m from each individual carbon group. Melting peaks of all AgSCn (n = 2−16) show similar values of fwhm (n = 2−16), regardless of chain length.

Solid-state ^{13}C NMR, in contrast, gives spatially specific details/clues of individual atoms/groups. As demonstrated in this section, the short-chain and odd/even effects are attributed to the different chemical environment of atoms at different locations of the alkyl chains, even though these atoms act collectively to yield a single calorimetric peak.

Linking calorimetry with ^{13}C NMR results is the key goal of this paper and will be discussed in section 3.5.

3.3.1. Chemical Shift (δ): Tagging Atomic Location and Degree of Conformation. Figure 4a shows the ^{13}C NMR spectra for all AgSCn (n = 1−16), with peaks assigned to particular locations of carbons based on prior studies.[38,53,73] These carbons can be categorized into three spatial segments along the alkyl chains, as summarized in Table 2: (1) head segment consisting of two atoms closest to the Ag−S slab; (2) mid-chain segment consisting of n − 5 CH_2 units with same chemical shift; (3) tail segment including the terminal three carbons closest to the interlayer interface. Carbons in the head and tail segments possess different chemical environment from that of the mid-chain groups.

Table 2. Three Segments of Alkyl Chains Deduced from ^{13}C NMR Analysis

segment	label	location	δ (ppm)
head	C-1	α-CH_2	39.5−41
head	C-2	β-CH_2	38.5−39.5
mid-chain		mid-chain CH_2	34−35.5
tail	Cn-2	penultimate CH_2	35−36
tail	Cn-1	outmost CH_2	25−26
tail	CH_3	terminal CH_3	14.5−20.5

The ∼34 ppm shift of the mid-chain units confirms their all-trans conformations,[74] as compared with the ∼30 ppm shift of n-alkanes in solution.[38,49] The ∼25 ppm shift of Cn-1 group is also a sign of all-trans chains.[49] This peak shifts to 22.1 ppm for AgSC4 with gauche defects[73] and 22.5 ppm for thiols in solution.[74] Chemical shifts of C-1 and C-2 of AgSCn (fwhm <75 Hz) are similar to those measured in thiol-capped Au nanoparticles, which, however, show broader peaks (fwhm ∼1020 Hz) due to the polydispersity of the S−(C-1) bonding in nanoparticles.[51,52]

3.3.2. Spin−Lattice Relaxation Time (T_1): Chain Mobility. Carbon spin−lattice relaxation time (T_1) is a sensitive indicator of local dynamics and molecular motions.[49,75] A shorter T_1 implies a larger mobility. Figure 4b shows the T_1 values of different carbon groups in AgSCn (n = 6, 8, 12). Groups that

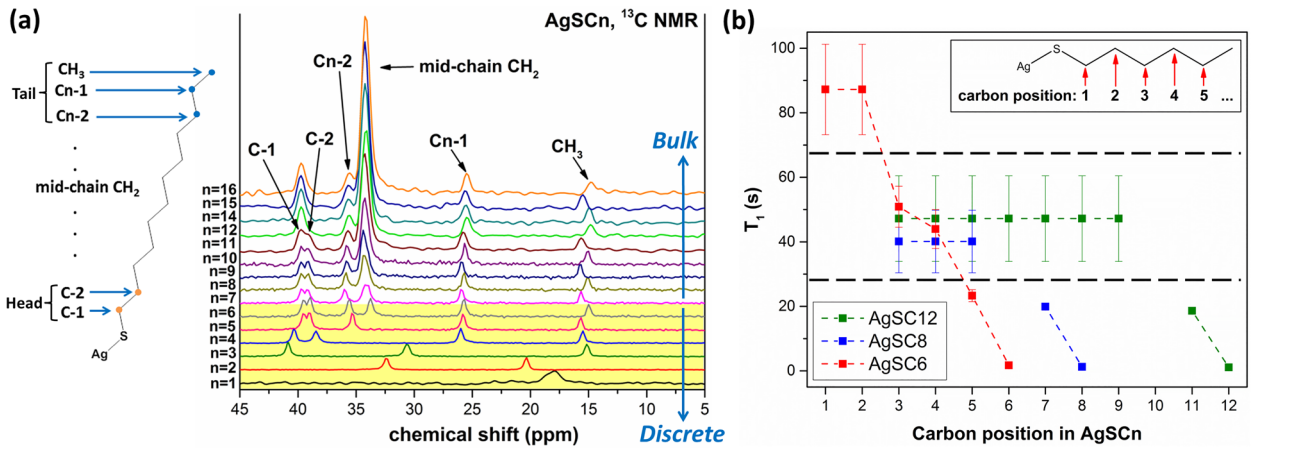

Figure 4. (a) Solid-state ^{13}C NMR (75.47 MHz) spectra for AgSCn (n = 1−16) lamellae. The schematic on the left shows the structure of one AgSCn molecule with labeled positions of carbon groups along the chain. (b) Plot shows T_1 values of carbon groups located at different positions along alkyl chains for AgSCn with n = 6, 8, 12.

DOI: 10.1021/acs.jpcc.7b03693
J. Phys. Chem. C 2017, 121, 13916−13929

are closer to the Ag−S slab are more restricted by chain tethering and thus less mobile (C-1 may not be involved in melting, section 3.5). Consistent with chemical shift, segmentation of alkyl chains (Table 2) can also be deduced from the differences in carbon mobility; T_1 of the head and the tail segments are, respectively, larger and smaller than that of the mid-chain units.

3.3.3. Mid-Chain CH_2 Groups (Bulk). The mid-chain ^{13}C NMR signal (Figure 4a) is only present in AgSC*n* of $n \geq 6$, with AgSC6 being the shortest species that contains mid-chain CH_2 units. Chemical shift and thus the chemical environment of mid-chain carbons, despite their local positions, are identical to that of bulk CH_2 units (32−35 ppm) in polyethylene[76,77] and long chain paraffins[55,78] and are independent of chain length (Figure 5, purple data points). Mid-chain CH_2 units exhibit bulk characteristics.

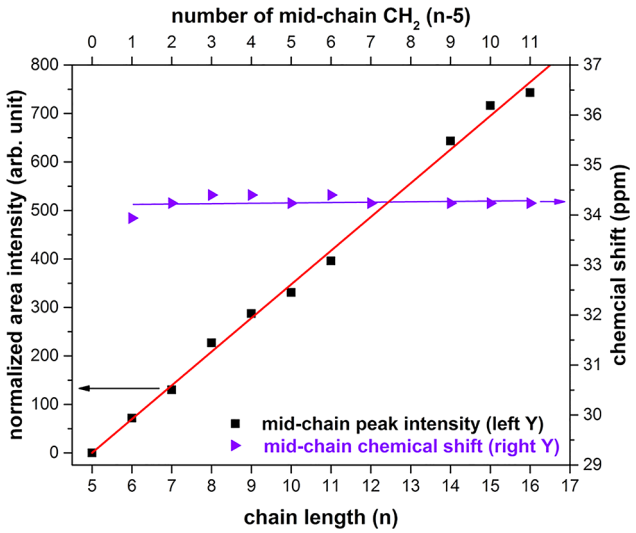

Figure 5. Plot shows the linear increase of the normalized area intensity (left *Y*-axis) and chemical shift (right *Y*-axis) of the mid-chain peaks as a function of chain length (bottom *X*-axis) and number of mid-chain groups (top *X*-axis).

There are "*n*" discrete peaks observed in the ^{13}C NMR spectra of AgSC*n* with $n \leq 6$; whereas at $n > 6$, no additional peak appears but the integrated intensity of the mid-chain peak linearly increases (Figure 5, black data points). Intensity values for AgSC*n* of $n \geq 7$ are multiple of that of AgSC6. This result can be semiquantitatively utilized to verify the number of mid-chain groups in alkyl chains.[49]

The attributes of mid-chain groups link the ^{13}C NMR and calorimetry results at $n \geq 6$. The simultaneous incremental change of both the mid-chain peak intensity (Figure 5, ~70 per CH_2) and the melting enthalpy (Figure 2b, $\Delta H_{CH_2} \approx 4.1$ kJ/mol per CH_2) indicates that the increase of chain length beyond AgSC6 is essentially elongating the total length of the bulk mid-chain segment.

3.3.4. Odd/Even Parity Effect of NMR Chemical Shift. Odd/even effect of chemical shift is observed in AgSC*n* by noting the oscillations of the ^{13}C NMR peaks of the three atoms in the tail segment (Figure 6 top plot): CH_3 ($\Delta\delta_{odd-even} \approx 0.7$ ppm), Cn-1 ($\Delta\delta_{odd-even} \approx 0.3$ ppm), and Cn-2 ($\Delta\delta_{odd-even} \approx 0.2$ ppm). Such oscillations are not found in the mid-chain or the head groups. Although the parity effect, if any, is also presented in the chemical shift of *n*-alkanes,[55] it is difficult to draw any

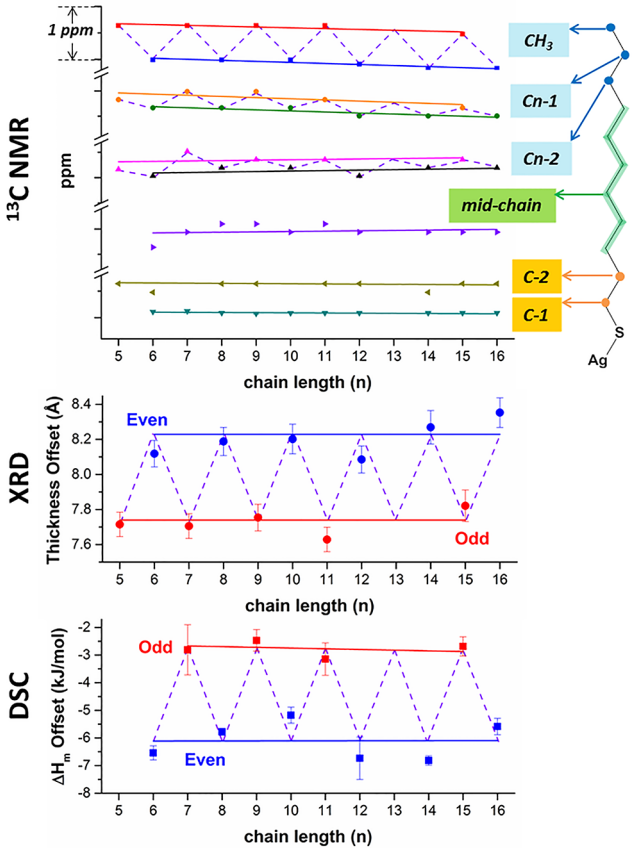

Figure 6. Top plot illustrates that the odd/even effect is observed in the NMR chemical shift of the CH_3, Cn-1, and Cn-2 groups but is absent in the mid-chain, C-2, and C-1 groups. For comparison, the middle and bottom plots show the odd/even effect measured in the layer thickness[2,13] offset and ΔH_m offset (calculated from Figure 2b) of AgSC*n* as a function of chain length, respectively.

conclusions since odd and even *n*-alkanes have different crystal structures.[79,80] In contrast, odd and even chain AgSC*n* (n = 2−16) share a same lattice packing.[13] Similar parity effect is also observed in the terminal CH_3 of metal alkanoate layers.[54,56]

3.3.4.1. Spatial Location. the odd/even effect of AgSC*n* is spatially confined to the interface region where adjacent lamella layers mate. The CH_3 groups undergo changes in chemical environment due to the difference of interlayer packing and odd/even variation of van der Waals gaps (Figure 6 middle plot).[13] The same spatial location of the parity effect was also obtained by comparing the melting of one-layer and stacked-layer (Figure 6 bottom plot) AgSC*n* [2] and thus quantitatively links the attributes independently measured from ^{13}C NMR, XRD,[13] and DSC.[2]

3.3.4.2. Strength and Depth of the Parity Effect. The odd/even effect not only is limited to the terminal CH_3 groups but extends into the lamella with a depth of three tail carbons (CH_3, Cn-1, Cn-2). These groups in odd chain AgSC*n* are more deshielded than in even chain AgSC*n* (Figure 6 top plot) while the strength of the parity effect progressively diminishes as their distances from the interlayer interface increase. Apparently, the redistribution of the charge density (chemical shift) along the chains due to the parity effect has a natural decay length (three tail atoms). This decay length is originated from the inductive effect of the CH_3 groups and the Ag−S slabs and will be discussed in section 4.1. It is notable that the

DOI: 10.1021/acs.jpcc.7b03693
J. Phys. Chem. C 2017, 121, 13916−13929

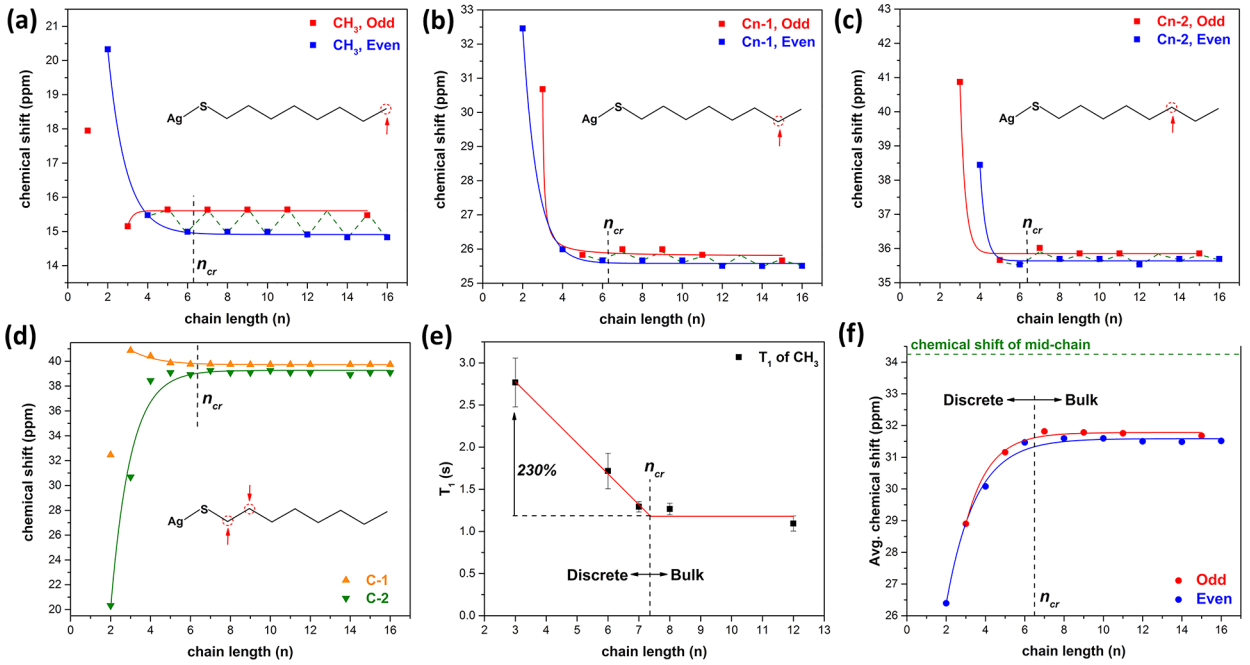

Figure 7. (a–d) Plots show the ^{13}C NMR chemical shift as a function of chain length for the terminal CH_3, Cn-1, Cn-2, and C-1 (orange) and C-2 (green) groups, respectively. (a)–(c) are plotted separately for odd and even AgSC*n*. (e) Plot shows the T_1 values of CH_3 groups as a function of chain length. The data points are fitted by a piecewise function ($T_1 = T_{1base}$ at $n \geq n_{cr}$; $T_1 = T_{1base} - k_1(n - n_{cr})$ at $n < n_{cr}$) that yields an $n_{cr} = 7.4 \pm 0.3$. (f) Plot shows the chemical shift value averaged by the number of ^{13}C NMR peaks for each AgSC*n* as a function of chain length. The green dashed line represents the chemical shift of mid-chain CH_2 groups.

number of tail groups is not a constant for all aliphatic layers; there are four tail atoms in *n*-alkanes as discussed in section 3.6.

3.3.5. Short-Chain Effect of NMR Chemical Shift and T_1. Short-chain effect of melting (T_m, ΔH_m) occurred below n_{cr} is the most intriguing finding of calorimetry data (section 3.1.3). Similar effect is also observed in the NMR chemical shift (Figure 7a–d) and T_1 values (Figure 7e) of certain carbons, with extraordinary changes as chain length reduces. They include (1) a ~50% reduction of the chemical shift of C-2, compared with the ~1% baseline noise level (Figure 7d), and (2) T_1 of the CH_3 group increases by as large as ~230% in the discrete AgSC*n* (n = 2–6, Figure 7e).

A critical chain length of $n_{cr} \approx 7$ is independently obtained from the chain-length dependence of chemical shift and T_1 values, consistent with that measured from calorimetry (sections 3.1.3 and 3.2). In the bulk range ($n \geq n_{cr}$), all parameters are fixed, while discrete changes of the data appear at $n < n_{cr}$.

Head and tail carbons in short chain AgSC*n* ($n < n_{cr}$) become untethered from their long chain values (Figure 7a–d). However, it is not straightforward to analyze the chemical shift of each atom due to label redundancy (e.g., C-2 and Cn-2 is the same atom in AgSC4).

A more revealing representation of the compound chemical environment is shown in Figure 7f, which illustrates the (unweighted) average chemical shift ($\bar{\delta}$) of all carbons in each AgSC*n*. This average value is fixed at 31–32 ppm (close to the bulk mid-chain value) in bulk AgSC*n* but decreases toward ~26 ppm in discrete AgSC*n*, with a progressively increased deviation from the bulk chemical shift. Chemical environment of discrete AgSC*n* ($n < n_{cr}$) is completely different from that of bulk, increasingly dominated by the tail and head segments.

3.4. Bulk-to-Discrete Transition. Aliphatic layers (e.g., alkanes, polyethylene) are often modeled as bulk alkyl chains sandwiched between 2D planes.[1,4,61] In AgSC*n*, these planes include the planar Ag–S sheet and the van der Waals interface (Figure 8a, left schematic).[2] A more realistic model considers the existence of Ag–S slabs and the interfaces as the causes for the chemical shift deviation of the head and tail segments from that of the bulk mid-chain carbons. The previous 2D planes are now assigned with 3D representations, each having a thickness determined by quantitative methods (Figure 8a, right schematic). The interface region contains the van der Waals gap and the tail segments from adjacent two layers; the Ag–S region includes the Ag–S slab and the two head segments tethered to it.

At $n \geq 7$, the Ag–S and the interface regions are distant from each other and act independently, with multiple *trans* mid-chain bonds between them (Figure 8b). Bulk melting (*trans* to *gauche* transition) only occurs when there is at least one mid-chain bond (i.e., two bulk mid-chain CH_2). Thus, bulk melting is not defined at $n \leq 6$ and melting of AgSC*n* starts to be anomalous, the occurrence of bulk-to-discrete transition. Critical length, n_{cr}, of aliphatic layers can be estimated from the sum of the sizes of the head (t_{head}) and tail (t_{tail}) segments as follows:

$$n_{cr} = t_{head} + t_{tail} + 2 \quad (4)$$

Notably, the estimated n_{cr} of *n*-alkane lamellae also satisfies eq 4, as reported in section 3.6. Figure 8c summarizes all the calorimetry and ^{13}C NMR results in this work that confirm n_{cr} = 7 in AgSC*n*.

3.5. Partial Atomic Assignment of ΔH_m: Linking DSC and ^{13}C NMR. ΔH_m measured by calorimetry is the composite value of the entire AgSC*n* lamellae. However, by using ^{13}C NMR, we attempt to deconvolute ΔH_m for the first time into contribution of every carbon in the chain, as illustrated by the assigned values in Figure 9 (n = 2–8). We suggest melting

DOI: 10.1021/acs.jpcc.7b03693
J. Phys. Chem. C 2017, 121, 13916–13929

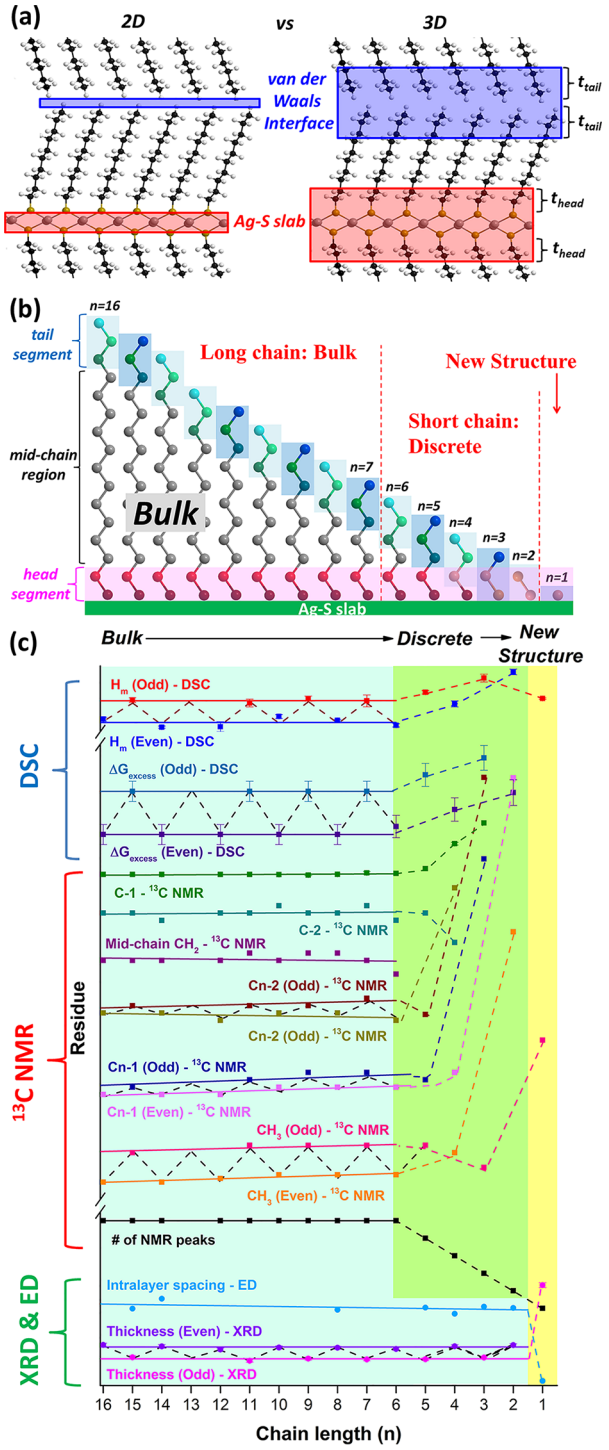

Figure 8. (a) Schematics visualize the 2D (left) and 3D (right) representations of the van der Waals interface (blue) and the Ag−S slab (red) in AgSC*n* layers. (b) Schematic visualizes the segmentation of alkyl chains in AgSC*n* (n = 2−16). Gray atoms: mid-chain region. Dark/light red atoms: different groups of head segment. Dark/light blue/green atoms: different groups of tail segment in odd/even chains. (c) Plot summarizes the structural and property parameters (by DSC, ^{13}C NMR, XRD, and electron diffraction) of AgSC*n* (n = 1−16) as the change of chain length. Each parameter is plotted as residue with regard to its linear fitting of certain bulk AgSC*n*. The thickness and intralayer spacing data are replotted from our prior paper[13] and are preserved all through n = 2−16.

enthalpy contributed from specific carbons changes with their chemical environment.

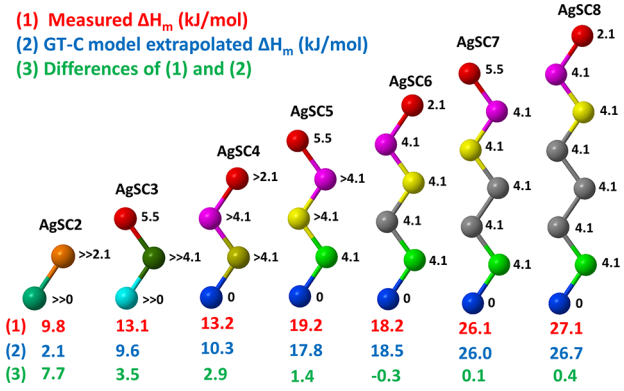

Figure 9. Cartoon shows the deconvolution of ΔH_m of AgSC*n* (n = 2−8) into contributions from each carbon (values beside carbons). The three rows of values represent (1) measured ΔH_m (Figure 2b), (2) ΔH_m extrapolated from GT-C linear fitting (Figure 2b), and (3) differences of (1) and (2).

From Voicu et al.'s variable-temperature NMR analysis,[38,39] we infer that C-1 does not undergo melting ($\Delta H_{C\text{-}1}$ = 0) in AgSC12 and AgSC18. Since no chemical shift variation is observed for C-1 at $n \geq 4$ (Figure 7d), we assign $\Delta H_{C\text{-}1}(n = 4\text{−}16) = 0$, whereas the assigned $\Delta H_{C\text{-}1}(n = 2, 3) > 0$.

Deduced from the extrapolation of long chain ΔH_m to n = 2 (Figure 2b), we obtain ΔH_{CH_3}(even) = 2.1 kJ/mol and ΔH_{CH_3}(odd) = 5.5 kJ/mol. All the other CH_2 groups contribute ΔH_{CH_2} = 4.1 kJ/mol. Variations observed in the chemical shift (Figure 7a−d) of specific carbons of AgSC*n* (n = 2−5) indicate alterations of their enthalpy contributions. Certain carbons in AgSC2 ($\Delta H_{C\text{-}1} + \Delta H_{CH_3}$ = 9.8 kJ/mol), AgSC3 ($\Delta H_{C\text{-}1} + \Delta H_{Cn\text{-}1}$ = 7.6 kJ/mol), AgSC4 ($\Delta H_{Cn\text{-}2} + \Delta H_{Cn\text{-}1} + \Delta H_{CH_3}$ = 13.2 kJ/mol), and AgSC5 ($\Delta H_{Cn\text{-}2} + \Delta H_{Cn\text{-}1}$ = 9.6 kJ/mol) contribute larger enthalpy than their counterparts in other AgSC*n*. We speculate the huge short-chain effect melting (e.g., 7.7 kJ/mol increase of ΔH_m in AgSC2) is originated from the unique chemical environment of these carbons.

3.6. Universal Rules of Chain Melting. Findings about the short-chain effect and parity effect are also generalized to the chain melting of other aliphatic lamellar crystals. Figure 10a replots the experimental T_m vs n curves of four such compounds: AgSC$_n$H$_{2n+1}$, CuSC$_n$H$_{2n+1}$ (CuSC*n*, copper alkanethiolate),[81] AuSC$_n$H$_{2n+1}$ (AuSC*n*, gold alkanethiolate),[82] and *n*-alkanes.[1,71] Modeling parameters of the latter three systems are summarized in Table 3. Figure S-5a−c and Figure 10b compare the experimental and modeled T_m of CuSC*n*, AuSC*n*, *n*-alkanes (n = 3−6001), and *n*-alkane (n = 3−20), respectively, with colored shades illustrating the degrees of the short-chain effect, similar to that of Figure 2a.

The GT-COM model well fits all the materials within acceptable errors. The absence of $\Delta G_{odd-even}$ for CuSC*n* and AuSCn is due to the lack of odd chain T_m data in literature.[81,82] Several observations are worth discussion.

Short-chain effect melting is observed in all aliphatic systems. Their T_m values deviate from the prediction of the GT-C model at $n < n_{cr}$, but each system has a different critical size of n_{cr}. This indicates that different lamellae have different lengths of head

DOI: 10.1021/acs.jpcc.7b03693
J. Phys. Chem. C 2017, 121, 13916−13929

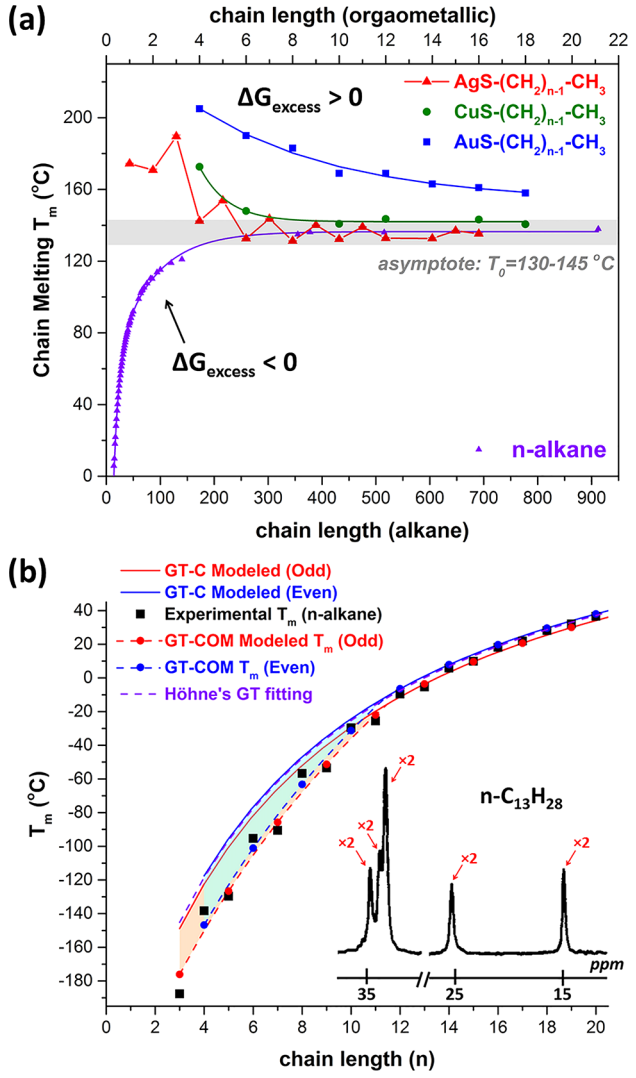

Figure 10. (a) Plot shows the T_m vs n for four aliphatic lamellar systems: n-alkane (purple),[1,71] AgSCn (red), CuSCn (green),[81] and AuSCn (blue).[82] The gray region represents the asymptotic T_m (130–145 °C) approached by all systems when $n \rightarrow \infty$. (b) Plot compares the experimental and modeled T_m vs n for n-alkane lamellae. The dashed red and blue curves are calculated by the GT-COM model. The solid red and blue curves refer to the GT-C model, in which the ΔG_{excess} term is assigned as the ΔG_{Base} of n-alkanes in Table 3. The orange and cyan shades visualize the deviations of the T_m from the GT-C model. The dashed purple curve refers to Höhne's GT-C fitting.[61] The inset replots the solid-state ^{13}C NMR spectrum of n-$C_{13}H_{28}$ lamellae.[55]

and/or tail segments. For example, n_{cr} = 11.48 revealed for n-alkanes infers that there are 5 pairs of nonequivalent carbon groups (i.e., 10 carbons) in n-decane, given the symmetric nature of n-alkane molecules. This demonstration is verified by the reported ^{13}C NMR result of $C_{10}H_{22}$, which shows 5 peaks.[83] These 5 peaks are maintained and the intensity of the mid-chain peak increases as chain length increases beyond n = 11 (e.g., $C_{13}H_{28}$, inset of Figure 10b),[55] whereas in C_8H_{18}, only four peaks are observed.[78] This is strong evidence for the validity of the chain segmentation.

Interestingly, short-chain effect of the well-known n-alkanes (Figure 10b) is undiscovered before, although the GT-C model has been applied to this system decades ago (e.g., purple curve in Figure 10b).[1,61,66,84] Since the GT-C model was usually employed for n-alkanes with chain lengths up to $n \approx 6000$, the short-chain deviations at $n \leq 11$ were easily buried when dealing with such large scale of chain lengths (Figure S-5c). Although the influence of lattice polymorphism, which appears especially at $n < 40$,[79,80] on T_m is suggested to be rather low for n-alkanes,[61] it can be another possible contribution to the T_m deviation in Figure 10b, besides the short-chain effect.

The sign of parameter k indicates whether the inorganic and/or the interface regions increase or decrease the total ΔG_{excess} of the system at $n < n_{cr}$ ($k = -d(\Delta G_{excess})/dn$). It determines the rate of T_m depression ($\Delta G_{excess} < 0$) or T_m enhancement ($\Delta G_{excess} > 0$) as chain length decreases. Figure S-5d summarizes the magnitude of ΔG_{excess} for the four materials discussed. The physical meaning of k is related to the overall inductive effect (Table 3, row 7) of different sources of ΔG_{excess} (e.g., interface, Ag–S, Au–S, or Cu–S) and is discussed in section 4.1.

Although different aliphatic lamellae may present different values of n_{cr}, k, $\Delta G_{odd-even}$, and $\Delta G_{odd-even}$, all of them show similar values of T_0; the asymptotic temperature of chain melting is always about 130–145 °C (gray area in Figure 10a). This indicates that any alkyl-based lamellar materials with very large chain lengths ($n \rightarrow \infty$) melt as if they were infinite bulk alkanes ($T_m \approx 140$ °C).[1]

4. DISCUSSION

The origin of the bulk-to-discrete transition is outside the scope of this work. Questions such as why the transition is abrupt in nature and why the ΔG_{excess} increases linearly as chain length decreases remain unclear. However, clues obtained from ^{13}C NMR and crystallography study indicate that nonuniform charge redistribution and lattice stress/strain may be responsible for the appearance of the short-chain effect.

4.1. Charge Redistribution and Inductive Effect.

Charge redistribution due to functional substituents is common in organic compounds, including the substituent effect in saturated chains or aromatic rings.[85−87] This effect is also observed for AgSCn by ^{13}C NMR in this work.

Chemical shift of carbon groups in a particular AgSCn follows a sequence of C-1 > C-2 > Cn-2 > mid-chain CH_2 > Cn-1 > CH_3 (Figure 4a), with electrons of C-1 mostly pulled

Table 3. GT-COM Modeling Results of Three Different Aliphatic Layered Materials

	$CuSC_nH_{2n+1}$	$AuSC_nH_{2n+1}$	n-alkanes
T_0 (°C)	142.3 ± 4.2	138.1 ± 1.9	141.8 ± 0.8
ΔG_{Base} (kJ/mol)	−0.043 ± 0.533	3.42 ± 0.26	−27.54 ± 0.39
$\Delta G_{odd-even}$ (kJ/mol)	NA	NA	−1.12 ± 0.33
n_{cr}	6.95 ± 0.78	8.73 ± 0.53	11.48 ± 0.47
k (kJ/mol)	−0.393 ± 0.078	0.235 ± 0.021	1.36 ± 0.14
overall inductive effect	electron-withdrawing	electron-releasing	electron-releasing

DOI: 10.1021/acs.jpcc.7b03693
J. Phys. Chem. C 2017, 121, 13916−13929

away. The superposition of two electrostatic effects is responsible for the observation: (1) the electron-withdrawing inductive effect[88−94] of the Ag−S slab; (2) the electron-releasing inductive effect[94,95] of CH_3 within the interfaces. Both effects propagate along chains but decay at distant groups.

The decay length employed in section 3.3.4 for the head and tail segments is originated from the diminishing distance of the inductive effect. The mid-chain carbons are hardly affected. Different aliphatic materials with specific functional groups (e.g., CH_3, Ag−S, Cu−S, Au−S) may have different decay lengths and thus different values of n_{cr} (eq 4). The value of parameter k is determined by the relative strength and directionality (electron-withdrawing or electron-releasing) of the overall inductive effect inherent in these functional groups (Table 3, row 7). This analysis provides a path of manipulating T_m of aliphatic layers by tailoring the function groups (e.g., AgSCn → AgSCn−OH, ΔT_m > 30 °C)[33] and has implications in biological membranes[31] and aliphatic electronics.[96−98]

We suggest S atoms in AgSCn are negatively charged ($q-$) while Ag and C are positively charged ($q+$).[99] Since chemical shift of carbons increases with positive partial charge (q),[91,93,99,100] the following expression is obtained:

$$(q+)_1 > (q+)_2 > (q+)_{n-2} > (q+)_{\text{mid-chain}} > (q+)_{n-1} > (q+)_n$$

Similar to silver alkanoate,[54] this charge distribution (Figure S-6a) is more nonuniform in short chain AgSCn ($n < n_{cr}$), with better resolved ^{13}C NMR peaks, than in long chain AgSCn. We speculate that electric dipoles (Figure S-6b) are induced between adjacent carbons, forming polar C−C bonds. Chain−chain van der Waals forces are essentially dipole−dipole interactions among the C−C, C−H, and C−S bonds all over layers. It is hypothesized that chains in short chain AgSCn are more strongly bound by such interactions so that extra energy is required to stimulate additional degrees of freedom at melting.

Therefore, computational study of melting enthalpy from chemical shift is possible and will be a focus of continued works. Henry et al. has utilized the ^{13}C NMR data to calculate the formation enthalpy of alkane.[100,101]

4.2. Stress/Strain of AgSCn Lattice. In our previous paper, we have verified that AgSCn with n = 2−16 share a common lattice structure.[13] Detailed lattice constants and space group of AgSCn will be reported in a future publication. However, slight lattice variations of 0.5−1.8% are observed when quantitatively comparing the structures of AgSC3 and AgSC15. This indicates a possible existence of stress/strain in the Ag−S slabs. Both the stress/strain[102,103] and the defects induced by stress/strain[104] can lead to variations of T_m.

5. CONCLUSION

We observed an abrupt bulk-to-discrete transition occurring at a critical chain length of n_{cr} = 7 in AgSCn (n = 1−16) layers, with extraordinary changes of chain melting properties, chemical environment, and relaxation time. Calorimetry and solid-state ^{13}C NMR are coupled to probe the global and local characteristics of atoms within the discrete regions of aliphatic lamellae.

Bulk (long chain) AgSCn ($n \geq 7$) exhibit fixed NMR chemical shift and T_1 values and size-dependent melting predictable by the classical GT model. In contrast, discrete (short chain) AgSCn (n = 2−6) present a short-chain effect, with completely different values of these parameters for every single change of chain length. None of the carbons share identical chemical environment. The anomalous melting is well-predicted by a new comprehensive GT model with variable ΔG_{excess}. AgSC1 is an outlier with a different crystal structure. A new 3D spatial model is constructed to divide the alkyl chains of AgSCn into two discrete (head, tail) and one bulk (mid-chain) segments. The discrete segments dominate the material at $n < n_{cr}$.

An odd/even effect is detected in both the melting and NMR chemical shift of AgSCn and is exclusively attributed to the nature of the tail segment.

This analysis is generalized to other extremely small aliphatic layers with discrete regions, including n-alkanes with $n_{cr} \approx 11$.

This finding is instructive to the design of novel alkyl-based layers with controllable properties (e.g., T_m), through the manipulation of molecular segments (e.g., interfacial groups). Potential applications include the optimization of molecular electronics and the study of biological membranes.

■ ASSOCIATED CONTENT

Supporting Information

The Supporting Information is available free of charge on the ACS Publications website at DOI: 10.1021/acs.jpcc.7b03693.

Additional characterization results and the detailed modeling procedure (PDF)

■ AUTHOR INFORMATION

Corresponding Author

*E-mail: l-allen9@illinois.edu.

ORCID

Leslie H. Allen: 0000-0001-9323-3767

Present Addresses

∥L.P.d.l.R.: SanDisk Corporation, Milpitas, CA 95035, U.S.

⊥Z.Y.: Lam Research Corporation, Fremont, CA 94538, U.S.

Notes

The authors declare no competing financial interest.

■ ACKNOWLEDGMENTS

This work is supported by Grants NSF-DMR-1409953 and NSF-DMR-1006385. Material characterizations were carried out in the NMR/EPR Laboratory, Frederick-Seitz Materials Research Laboratory and Ceramics Kiln House at the University of Illinois, Urbana—Champaign. The authors thank Prof. P. Braun, Prof. S. Zimmerman, Prof. J. J. Cheng, Prof. K. Schweizer, Prof. J. M. Zuo, and Prof. J. Lyding for discussions. We also thank N. Robards for help with calorimetry measurements.

■ REFERENCES

(1) Wunderlich, B.; Czornyj, G. A Study of Equilibrium Melting of Polyethylene. *Macromolecules* **1977**, *10*, 906−913.

(2) de la Rama, L. P.; Hu, L.; Ye, Z.; Efremov, M. Y.; Allen, L. H. Size Effect and Odd-Even Alternation in the Melting of Single and Stacked Agscn Layers: Synthesis and Nanocalorimetry Measurements. *J. Am. Chem. Soc.* **2013**, *135*, 14286−14298.

(3) Uchida, Y.; Nishizawa, T.; Omiya, T.; Hirota, Y.; Nishiyama, N. Nanosheet Formation in Hyperswollen Lyotropic Lamellar Phases. *J. Am. Chem. Soc.* **2016**, *138*, 1103−1105.

(4) Hoffman, J.; Weeks, J. Melting Process and the Equilibrium Melting Temperature of Polychlorotrifluoroethylene. *J. Res. Natl. Bur. Stand., Sect. A* **1962**, *66A*, 13−28.

DOI: 10.1021/acs.jpcc.7b03693
J. Phys. Chem. C 2017, 121, 13916−13929

(5) Buffat, P.; Borel, J. P. Size Effect on Melting Temperature of Gold Particles. *Phys. Rev. A: At., Mol., Opt. Phys.* **1976**, *13*, 2287−2298.
(6) Coombes, C. J. The Melting of Small Particles of Lead and Indium. *J. Phys. F: Met. Phys.* **1972**, *2*, 441−9.
(7) Zhang, M.; Efremov, M. Y.; Schiettekatte, F.; Olson, E. A.; Kwan, A. T.; Lai, S. L.; Wisleder, T.; Greene, J. E.; Allen, L. H. Size-Dependent Melting Point Depression of Nanostructures: Nanocalorimetric Measurements. *Phys. Rev. B: Condens. Matter Mater. Phys.* **2000**, *62*, 10548−10557.
(8) Arvizo, R. R.; Miranda, O. R.; Thompson, M. A.; Pabelick, C. M.; Bhattacharya, R.; Robertson, J. D.; Rotello, V. M.; Prakash, Y. S.; Mukherjee, P. Effect of Nanoparticle Surface Charge at the Plasma Membrane and Beyond. *Nano Lett.* **2010**, *10*, 2543−2548.
(9) Verma, A.; Stellacci, F. Effect of Surface Properties on Nanoparticle−Cell Interactions. *Small* **2010**, *6*, 12−21.
(10) Dorset, D. L.; Moss, B.; Wittmann, J. C.; Lotz, B. The Pre-Melt Phase of N-Alkanes: Crystallographic Evidence for a Kinked Chain Structure. *Proc. Natl. Acad. Sci. U. S. A.* **1984**, *81*, 1913−1917.
(11) Lai, S. L.; Guo, J. Y.; Petrova, V.; Ramanath, G.; Allen, L. H. Size-Dependent Melting Properties of Small Tin Particles: Nanocalorimetric Measurements. *Phys. Rev. Lett.* **1996**, *77*, 99−102.
(12) Majumder, C.; Kumar, V.; Mizuseki, H.; Kawazoe, Y. Small Clusters of Tin: Atomic Structures, Energetics, and Fragmentation Behavior. *Phys. Rev. B: Condens. Matter Mater. Phys.* **2001**, *64*, 233405.
(13) Ye, Z.; de la Rama, L. P.; Efremov, M. Y.; Zuo, J.-M.; Allen, L. H. Approaching the Size Limit of Organometallic Layers: Synthesis and Characterization of Highly Ordered Silver-Thiolate Lamellae with Ultra-Short Chain Lengths. *Dalton Trans.* **2016**, *45*, 18954−18966.
(14) Mak, K. F.; Lee, C.; Hone, J.; Shan, J.; Heinz, T. F. Atomically Thin Mos2: A New Direct-Gap Semiconductor. *Phys. Rev. Lett.* **2010**, *105*, 136805.
(15) Zhang, Y.; et al. Crossover of the Three-Dimensional Topological Insulator Bi2se3 to the Two-Dimensional Limit. *Nat. Phys.* **2010**, *6*, 584−588.
(16) Hong, S. S.; Kundhikanjana, W.; Cha, J. J.; Lai, K.; Kong, D.; Meister, S.; Kelly, M. A.; Shen, Z.-X.; Cui, Y. Ultrathin Topological Insulator Bi2se3 Nanoribbons Exfoliated by Atomic Force Microscopy. *Nano Lett.* **2010**, *10*, 3118−3122.
(17) Cha, S.-H.; Kim, J.-U.; Kim, K.-H.; Lee, J.-C. Preparation and Photoluminescent Properties of Gold(I)-Alkanethiolate Complexes Having Highly Ordered Supramolecular Structures. *Chem. Mater.* **2007**, *19*, 6297−6303.
(18) Novoselov, K. S.; Geim, A. K.; Morozov, S. V.; Jiang, D.; Zhang, Y.; Dubonos, S. V.; Grigorieva, I. V.; Firsov, A. A. Electric Field Effect in Atomically Thin Carbon Films. *Science* **2004**, *306*, 666−669.
(19) Wang, Q. H.; Kalantar-Zadeh, K.; Kis, A.; Coleman, J. N.; Strano, M. S. Electronics and Optoelectronics of Two-Dimensional Transition Metal Dichalcogenides. *Nat. Nanotechnol.* **2012**, *7*, 699−712.
(20) Hu, L.; de la Rama, L. P.; Efremov, M. Y.; Anahory, Y.; Schiettekatte, F.; Allen, L. H. Synthesis and Characterization of Single-Layer Silver Decanethiolate Lamellar Crystals. *J. Am. Chem. Soc.* **2011**, *133*, 4367−4376.
(21) Jadzinsky, P. D.; Calero, G.; Ackerson, C. J.; Bushnell, D. A.; Kornberg, R. D. Structure of a Thiol Monolayer-Protected Gold Nanoparticle at 1.1 Angstrom Resolution. *Science* **2007**, *318*, 430−433.
(22) Shvartsburg, A. A.; Jarrold, M. F. Solid Clusters above the Bulk Melting Point. *Phys. Rev. Lett.* **2000**, *85*, 2530−2532.
(23) Breaux, G. A.; Benirschke, R. C.; Sugai, T.; Kinnear, B. S.; Jarrold, M. F. Hot and Solid Gallium Clusters: Too Small to Melt. *Phys. Rev. Lett.* **2003**, *91*, 215508.
(24) Breaux, G. A.; Neal, C. M.; Cao, B.; Jarrold, M. F. Melting, Premelting, and Structural Transitions in Size-Selected Aluminum Clusters with around 55 Atoms. *Phys. Rev. Lett.* **2005**, *94*, 173401.
(25) Lai, S. L.; Carlsson, J. R. A.; Allen, L. H. Melting Point Depression of Al Clusters Generated During the Early Stages of Film Growth: Nanocalorimetry Measurements. *Appl. Phys. Lett.* **1998**, *72*, 1098−1100.
(26) Efremov, M. Y.; Schiettekatte, F.; Zhang, M.; Olson, E. A.; Kwan, A. T.; Berry, R. S.; Allen, L. H. Discrete Periodic Melting Point Observations for Nanostructure Ensembles. *Phys. Rev. Lett.* **2000**, *85*, 3560−3563.
(27) Olson, E. A.; Efremov, M. Y.; Zhang, M.; Zhang, Z. S.; Allen, L. H. Size-Dependent Melting of Bi Nanoparticles. *J. Appl. Phys.* **2005**, *97*, 034304.
(28) Sun, J.; Simon, S. L. The Melting Behavior of Aluminum Nanoparticles. *Thermochim. Acta* **2007**, *463*, 32−40.
(29) Reiss, H.; Wilson, I. B. The Effect of Surface on Melting Point. *J. Colloid Sci.* **1948**, *3*, 551−561.
(30) Sakai, H. Surface-Induced Melting of Small Particles. *Surf. Sci.* **1996**, *351*, 285−291.
(31) Chapman, D.; Urbina, J.; Keough, K. M. Biomembrane Phase Transitions: Studies of Lipid-Water Systems Using Differential Scanning Calorimetry. *J. Biol. Chem.* **1974**, *249*, 2512−2521.
(32) Mohwald, H. Phospholipid and Phospholipid-Protein Monolayers at the Air/Water Interface. *Annu. Rev. Phys. Chem.* **1990**, *41*, 441−476.
(33) Ye, Z.; Efremov, M. Y.; De la Rama, L. P.; Allen, L. H. Manuscript in preparation.
(34) Theodoratou, A.; Jonas, U.; Loppinet, B.; Geue, T.; Stangenberg, R.; Keller, R.; Li, D.; Berger, R. d.; Vermant, J.; Vlassopoulos, D. Semifluorinated Alkanes at the Air-Water Interface: Tailoring Structure and Rheology at the Molecular Scale. *Langmuir* **2016**, *32*, 3139−3151.
(35) Thomas, P. J.; Lavanya, A.; Sabareesh, V.; Kulkarni, G. U. Self-Assembling Bilayers of Palladiumthiolates in Organic Media. *Proc. - Indian Acad. Sci., Chem. Sci.* **2001**, *113*, 611−619.
(36) Baena, M. J.; Espinet, P.; Lequerica, M. C.; Levelut, A. M. Mesogenic Behavior of Silver Thiolates with Layered Structure in the Solid-State - Covalent Soaps. *J. Am. Chem. Soc.* **1992**, *114*, 4182−4185.
(37) Bardeau, J.-F. o.; Parikh, A. N.; Beers, J. D.; Swanson, B. I. Phase Behavior of a Structurally Constrained Organic-Inorganic Crystal: Temperature-Dependent Infrared Spectroscopy of Silver N-Dodecanethiolate. *J. Phys. Chem. B* **2000**, *104*, 627−635.
(38) Voicu, R.; Badia, A.; Morin, F.; Lennox, R. B.; Ellis, T. H. Thermal Behavior of a Self-Assembled Silver N-Dodecanethiolate Layered Material Monitored by Dsc, Ftir, and ^{13}c Nmr Spectroscopy. *Chem. Mater.* **2000**, *12*, 2646−2652.
(39) Voicu, R.; Badia, A.; Morin, F.; Lennox, R. B.; Ellis, T. H. Structure and Dynamics of Selectively Deuterated Self-Assembled Silver N-Octadecanethiolate Layerered Materials. *Chem. Mater.* **2001**, *13*, 2266−2271.
(40) Levchenko, A. A.; Yee, C. K.; Parikh, A. N.; Navrotsky, A. Energetics of Self-Assembly and Chain Confinement in Silver Alkanethiolates: Enthalpy-Entropy Interplay. *Chem. Mater.* **2005**, *17*, 5428−5438.
(41) Marsh, D. General Features of Phospholipid Phase Transitions. *Chem. Phys. Lipids* **1991**, *57*, 109−120.
(42) Nagle, J. F. Theory of the Main Lipid Bilayer Phase Transition. *Annu. Rev. Phys. Chem.* **1980**, *31*, 157−196.
(43) Mouritsen, O. G. Theoretical Models of Phospholipid Phase Transitions. *Chem. Phys. Lipids* **1991**, *57*, 179−194.
(44) de la Rama, L. P.; Hu, L.; Efremov, M. Y.; Olson, E. A.; Nealey, P. F.; McLean, M. A.; Sligar, S. G.; Allen, L. H. Anomalous Transitions of Dodab Using Fast Scanning Liquid Calorimetry. *Thermochim. Acta* **2011**, *522*, 72−76.
(45) Hill, M. W. The Effect of Anaesthetic-Like Molecules on the Phase Transition in Smectic Mesophases of Dipalmitoyllecithin I. The Normal Alcohol up to C = 9 and Three Inhalation Anaesthetics. *Biochim. Biophys. Acta, Biomembr.* **1974**, *356*, 117−124.
(46) Trauble, H.; Eibl, H.; Sawada, H. Respiration - a Critical Phenomenon? *Naturwissenschaften* **1974**, *61*, 344−354.
(47) Eliasz, A. W.; Chapman, D.; Ewing, D. F. Phospholipid Phase Transitions. Effects of N-Alcohols, N-Monocarboxylic Acids, Phenylalkyl Alcohols and Quatenary Ammonium Compounds. *Biochim. Biophys. Acta, Biomembr.* **1976**, *448*, 220−233.

DOI: 10.1021/acs.jpcc.7b03693
J. Phys. Chem. C 2017, 121, 13916−13929

(48) Gao, W.; Reven, L. Solid-State Nmr Studies of Self-Assembled Monolayers. *Langmuir* **1995**, *11*, 1860−1863.
(49) Badia, A.; Gao, W.; Singh, S.; Demers, L.; Cuccia, L.; Reven, L. Structure and Chain Dynamics of Alkanethiol-Capped Gold Colloids. *Langmuir* **1996**, *12*, 1262−1269.
(50) Badia, A.; Singh, S.; Demers, L.; Cuccia, L.; Brown, G. R.; Lennox, R. B. Self-Assembled Monolayers on Gold Nanoparticles. *Chem. - Eur. J.* **1996**, *2*, 359−363.
(51) Badia, A.; Cuccia, L.; Demers, L.; Morin, F.; Lennox, R. B. Structure and Dynamics in Alkanethiolate Monolayers Self-Assembled on Gold Nanoparticles: A Dsc, Ft-Ir, and Deuterium Nmr Study. *J. Am. Chem. Soc.* **1997**, *119*, 2682−2692.
(52) Badia, A.; Demers, L.; Dickinson, L.; Morin, F. G.; Lennox, R. B.; Reven, L. Gold-Sulfur Interactions in Alkylthiol Self-Assembled Monolayers Formed on Gold Nanoparticles Studied by Solid-State Nmr. *J. Am. Chem. Soc.* **1997**, *119*, 11104−11105.
(53) Bensebaa, F.; Ellis, T. H.; Kruus, E.; Voicu, R.; Zhou, Y. Characterization of Self-Assembled Bilayers: Silver-Alkanethiolates. *Langmuir* **1998**, *14*, 6579−6587.
(54) Nelson, P. N.; Ellis, H. A. Structural, Odd-Even Chain Alternation and Thermal Investigation of a Homologous Series of Anhydrous Silver(I) N-Alkanoates. *Dalton Trans.* **2012**, *41*, 2632−2638.
(55) Imashiro, F.; Maeda, T.; Nakai, T.; Saika, A.; Terao, T. Chain-Length-Dependent Carbon-13 Nmr Chemical Shifts of N-Alkanes in Urea Inclusion Compounds. *J. Phys. Chem.* **1986**, *90*, 5498−5500.
(56) Nelson, P. N.; Ellis, H. A.; Taylor, R. A. Odd-Even Alternation in a Homologous Series of Zn (Ii) N-Alkanoates. *J. Mol. Struct.* **2011**, *986*, 10−15.
(57) Ye, Z.; de la Rama, L. P.; Hu, L.; Efremov, M. Y.; Allen, L. H. Nanocalorimetry Study of the Evolution of Melting Characteristics of Single Layer Silver Alkanethiolate Lamella: Fast Heating/Cooling and Electrical Annealing. *Thermochim. Acta* **2015**, *603*, 69−78.
(58) Thomson, J. J. *Application of Dynamics to Physics and Chemistry*; McMillan: London, 1888.
(59) Pawlow, P. Ober die Abhängigkeit des Schmelzpunktes von der Oberflächenenergie eines festen Körpers (Zusatz.). *Z. Phys. Chem.* **1909**, *65*, 545.
(60) Hoffman, J. D.; Weeks, J. J. X-Ray Study of Isothermal Thickening of Lamellae in Bulk Polyethylene at the Crystallization Temperature. *J. Chem. Phys.* **1965**, *42*, 4301−4302.
(61) Hohne, G. W. H. Another Approach to the Gibbs-Thomson Equation and the Melting Point of Polymers and Oligomers. *Polymer* **2002**, *43*, 4689−4698.
(62) Barybin, A.; Shapovalov, V. Modification of Pawlow's Thermodynamical Model for the Melting of Small Single-Component Particles. *J. Appl. Phys.* **2011**, *109*, 034303.
(63) Takagi, M. Electron-Diffraction Study of Liquid-Solid Transition of Thin Metal Films. *J. Phys. Soc. Jpn.* **1954**, *9*, 359.
(64) Lauritzen, J.; Hoffman, J. Formation of Polymer Crystals with Folded Chains from Dilute Solution. *J. Chem. Phys.* **1959**, *31*, 1680.
(65) Lauritzen, J.; Hoffman, J. Theory of Formation of Polymer Crystals with Folded Chains in Dilute Solution. *J. Res. Natl. Bur. Stand., Sect. A* **1960**, *64A*, 73−102.
(66) Hohne, G. W. H. Calorimetry on Small Systems-a Thermodynamic Contribution. *Thermochim. Acta* **2003**, *403*, 25−36.
(67) Denton, A. R.; Ashcroft, N. W. Vegard's Law. *Phys. Rev. A: At., Mol., Opt. Phys.* **1991**, *43*, 3161−3164.
(68) Wei, H.; Li, M.; Ye, Z.; Yang, Z.; Zhang, Y. Novel Ga-Doped Zno Nanocrystal Ink: Synthesis and Characterization. *Mater. Lett.* **2011**, *65*, 427−429.
(69) Wei, H.; Ye, Z.; Li, M.; Su, Y.; Yang, Z.; Zhang, Y. Tunable Band Gap Cu2znsns4xse4(1-X) Nanocrystals: Experimental and First-Principles Calculations. *CrystEngComm* **2011**, *13*, 2222−2226.
(70) Quinn, F., Jr.; Mandelkern, L. Additions and Corrections: Thermodynamics of Crystallization in High Polymers: Polyethylene. *J. Am. Chem. Soc.* **1959**, *81*, 6533−6533.
(71) Himran, S.; Suwono, A.; Mansoori, G. A. Characterization of Alkanes and Paraffin Waxes for Application as Phase Change Energy Storage Medium. *Energy Sources* **1994**, *16*, 117−128.
(72) Mori, A.; Maruyama, M.; Furukawa, Y. Second-Order Expansion of Gibbs-Thomson Equation and Melting Point Depression of Ice Crystallite. *J. Phys. Soc. Jpn.* **1996**, *65*, 2742−2744.
(73) Fijolek, H. G.; Grohal, J. R.; Sample, J. L.; Natan, M. J. A Facile Trans to Gauche Conversion in Layered Silver Butanethiolate. *Inorg. Chem.* **1997**, *36*, 622−628.
(74) Earl, W. L.; VanderHart, D. L. Observations in Solid Polyethylenes by Carbon-13 Nuclear Magnetic Resonance with Magic Angle Sample Spinning. *Macromolecules* **1979**, *12*, 762−767.
(75) Zeigler, R. C.; Maciel, G. E. Study of Dimethyloctadecylsilyl-Modified Silica Using Solid-State Carbon-13 Lineshapes and Relaxation Techniques. *J. Phys. Chem.* **1991**, *95*, 7345−7353.
(76) Piche, L.; Daigle, J.-C.; Claverie, J. P. A Ruthenium Catalyst Yielding Crosslinked Polyethylene. *Chem. Commun.* **2011**, *47*, 7836−7838.
(77) Galland, G. B.; de Souza, R. F.; Mauler, R. S.; Nunes, F. F. ^{13}c Nmr Determination of the Composition of Linear Low-Density Polyethylene Obtained with [H^3-Methallyl-Nickel-Diimine]Pf_6 Complex. *Macromolecules* **1999**, *32*, 1620−1625.
(78) Lindeman, L. P.; Adama, J. Q. Carbon-13 Nuclear Magnetic Resonance Spectrometry. Chemical Shifts for the Paraffins through C9. *Anal. Chem.* **1971**, *43*, 1245−1252.
(79) Boese, R.; Weiss, H.-C.; Blaser, D. The Melting Point Alternation in the Short-Chain N-Alkanes: Single-Crystal X-Ray Analyses of Propane at 30 K and of N-Butane to N-Nonane at 90 K. *Angew. Chem., Int. Ed.* **1999**, *38*, 988−992.
(80) Dorset, D. L. *Crystallography of the Polymethylene Chain*, 1st ed.; Oxford University Press: New York, 2005; pp 33−45.
(81) Espinet, P.; Lequerica, M. C.; Martín-Alvarez, J. M. Synthesis, Structural Characterization and Mesogenic Behavior of Copper(I) N-Alkylthiolates. *Chem. - Eur. J.* **1999**, *5*, 1982−1986.
(82) Cha, S.-H.; Kim, K.-H.; Kim, J.-U.; Lee, W.-K.; Lee, J.-C. Thermal Behavior of Gold(I)-Thiolate Complexes and Their Transformation into Gold Nanoparticles under Heat Treatment Process. *J. Phys. Chem. C* **2008**, *112*, 13862−13868.
(83) Chemical Book CAS Database List. http://www.chemicalbook.com/CASDetailList_19500_EN.htm (accessed Feb 15, 2017).
(84) Broadhurst, M. G. An Analysis of the Solid Phase Behavior of the Normal Paraffins. *J. Res. Natl. Bur. Stand., Sect. A* **1962**, *66A*, 241.
(85) Hendrickson, J. B. *Organic Chemistry*, 3rd ed.; McGraw-Hill: New York, 1970.
(86) Topsom, R. D. The Nature and Analysis of Substituent Electronic Effects. In *Progress in Physical Organic Chemistry*; Taft, R. W., Ed.; John Wiley & Sons, Inc., 1976; Vol. *12*, pp 1−19, DOI: 10.1002/9780470171912.ch1.
(87) Stock, L. M. The Origin of the Inductive Effect. *J. Chem. Educ.* **1972**, *49*, 400.
(88) Ingold, C. K. *Structure and Mechanism in Organic Chemistry*; Cornell University Press: New York, 1953.
(89) Spiesecke, H.; Schneider, W. G. Effect of Electronegativity and Magnetic Anisotropy of Substituents on C13 and H1 Chemical Shifts in Ch3x and Ch3ch2x Compounds. *J. Chem. Phys.* **1961**, *35*, 722−731.
(90) Pople, J. A.; Gordon, M. Molecular Orbital Theory of the Electronic Structure of Organic Compounds. I. Substituent Effects and Dipole Moments. *J. Am. Chem. Soc.* **1967**, *89*, 4253−4261.
(91) Farnum, D. G.; Gold, V. Charge Density-NMR Chemical Shift Correlations in Organic Ions. In *Advances in Physical Organic Chemistry*; Academic Press, 1975; Vol. *11*, pp 123−175, DOI: 10.1016/S0065-3160(08)60341-X.
(92) Morishima, I.; Yoshikawa, K.; Okada, K.; Yonezawa, T.; Goto, K. Conformational Dependence of the Inductive Effect in The .Sigma.-Electron System as Studied by Carbon-13 Nuclear Magnetic Resonance. *J. Am. Chem. Soc.* **1973**, *95*, 165−171.
(93) Fliszar, S. Charge Distributions and Chemical Effects. Xii. A Unifying Concept. *Can. J. Chem.* **1976**, *54*, 2839−2846.

DOI: 10.1021/acs.jpcc.7b03693
J. Phys. Chem. C 2017, 121, 13916−13929

(94) Roberts, J. D.; Caserio, M. C. *Basic Principles of Organic Chemistry*; Benjamin Inc.: New York, 1965.
(95) Bassindale, A. R.; Eaborn, C.; Walton, D. R. M.; Young, D. J. The Electron-Releasing Effects of Mono-, Bis-, and Tris-(Trimethylsilyl)Methyl Groups. The Importance of Hyperconjugation in the Electronic Effects of A-Metalloalkyl Groups. *J. Organomet. Chem.* **1969**, *20*, 49−56.
(96) John, N. S.; Pati, S. K.; Kulkarni, G. U. Electrical Characteristics of Layered Palladium Alkanethiolates by Conducting Atomic Force Microscopy. *Appl. Phys. Lett.* **2008**, *92*, 013120.
(97) Popoff, R. T. W.; Zavareh, A. A.; Kavanagh, K. L.; Yu, H.-Z. Reduction of Gold Penetration through Phenyl-Terminated Alkyl Monolayers on Silicon. *J. Phys. Chem. C* **2012**, *116*, 17040−17047.
(98) Popoff, R. T. W.; Kavanagh, K. L.; Yu, H.-Z. Preparation of Ideal Molecular Junctions: Depositing Non-Invasive Gold Contacts on Molecularly Modified Silicon. *Nanoscale* **2011**, *3*, 1434−1445.
(99) Fliszar, S.; Goursot, A.; Dugas, H. Charge Distribution and Chemical Effects. V. Modified Population Analysis. Application to Carbon-13 Nuclear Magnetic Resonance Shifts. *J. Am. Chem. Soc.* **1974**, *96*, 4358−4363.
(100) Henry, H.; Fliszar, S. Charge Distributions and Chemical Effects. 13. Ab Initio Study of the Charge Density-Carbon-13 Nuclear Magnetic Resonance Shift Correlation for Ethylenic Carbon Atoms. *J. Am. Chem. Soc.* **1978**, *100*, 3312−3315.
(101) Henry, H.; Fliszar, S.; Julg, A. Charge Distributions and Chemical Effects. X. Enthalpies of Formation of Alkanes, a Calculation from 13c Nuclear Magnetic Resonance Shifts. *Can. J. Chem.* **1976**, *54*, 2085−2088.
(102) Levitas, V. I.; Henson, B. F.; Smilowitz, L. B.; Asay, B. W. Solid-Solid Phase Transformation Via Internal Stress-Induced Virtual Melting, Significantly Below the Melting Temperature. Application to Hmx Energetic Crystal. *J. Phys. Chem. B* **2006**, *110*, 10105−10119.
(103) Hwang, Y. S.; Levitas, V. I. Internal Stress-Induced Melting Below Melting Temperature at High-Rate Laser Heating. *Appl. Phys. Lett.* **2014**, *104*, 263106.
(104) Fecht, H. J. Defect-Induced Melting and Solid-State Amorphization. *Nature* **1992**, *356*, 133−135.

DOI: 10.1021/acs.jpcc.7b03693
J. Phys. Chem. C 2017, 121, 13916−13929